Terrestrial, Atmospheric and Oceanic Sciences

RESEARCH Open Access

Fast report: preliminary analysis of coseismic landslides in the 2025 M6.4 Dapu earthquake

Yi-Yu Li[1,2*], Chun-En Lin[2*] and Chen-Yu Chen[2]

Abstract
After the 2025 M6.4 Dapu earthquake, the Agency of Rural Development and Soil and Water Conservation (ARDSWC) identified 29 coseismic landslides using Sentinel-2 and PlanetScope satellite imagery. Two-thirds of these landslides occurred south of the epicenter, indicating a likely southward rupture. These landslides are found to (1) locate in areas where PGA exceeded 250 cm/s^2 and PGV over 17 cm/s (2) occur on 30° to 50° slopes, often on southeast- to southwest-facing aspects. Dip slopes and the reactivation of historical landslides were key contributing factors. Although satellite imagery detected fewer landslides than other earthquakes with comparable magnitude, our field surveys revealed numerous fresh landslide scarps in areas with PGA over 400 cm/s^2 and PGV around 30 cm/s. Our analysis provides useful information of coseismic landslide behaviors and the triggering factors in the Dapu event. These findings highlight the importance of detailed post-earthquake landslide mapping and field investigations, which provides key information for advanced hazard mitigation plans for seismically affected regions in preparation for the upcoming rainy season.

Keywords Dapu earthquake, Coseismic landslides, Directivity effect, Topographic site effect, Earthquake legacy effect

1 Introduction

The M6.4 Dapu earthquake struck southwestern Taiwan on January 20, 2025, at 16:17 (UTC). The hypocenter was at 23.22°N, 120.55°E with a focal depth of 15.8 km, according to the earthquake archived report from the Central Weather Administration (CWA) (https://scweb.cwa.gov.tw/zh-tw/earthquake/details/20250121001726 64007). The focal mechanism from the AutoBATS CMT Catalog (Jian et al. 2018; Heidbach et al. 2022) (https://tecdc.earth.sinica.edu.tw/FM/AutoBATS/) revealed that the Dapu earthquake was a thrusting-faulting event. Recent studies indicate that the regions southwest of the epicenter experienced the largest coseismic slip, with maximum slip of 27.9 cm on the fault plane (Lee et al. 2025a), and 7 cm line-of-sights (LOS) displacements from interferometric synthetic aperture radar (InSAR) (Lee et al. 2025b). Wu et al. (2025) also showed that the southwestern region experienced the strongest ground shaking with PGA over 400 cm/s^2 and PGV above 30 cm/s.

Furthermore, this region is highly overlapped with the Geologically Sensitive Area with Landslide from the Geological Survey and Mining Management Agency (GSMMA), which means that this area is at high risk of being affected by landslides. Thus, detailed investigation of the geological hazards after the Dapu earthquake is important because coseismic landslides often cause significant economic loss and pose serious threats to human life (Keefer 1984). Studies have shown that a magnitude 6.4 earthquake is capable of triggering quite a few coseismic landslides (Malamud et al. 2004; Tanyaş and

*Correspondence:
Yi-Yu Li
joseliyiyu@gmail.com
Chun-En Lin
jasonsinlin@gmail.com
[1]Agricultural Technology Research Institute, Hsinchu, Taiwan
[2]Agency of Rural Development and Soil and Water Conservation, Nantou, Taiwan

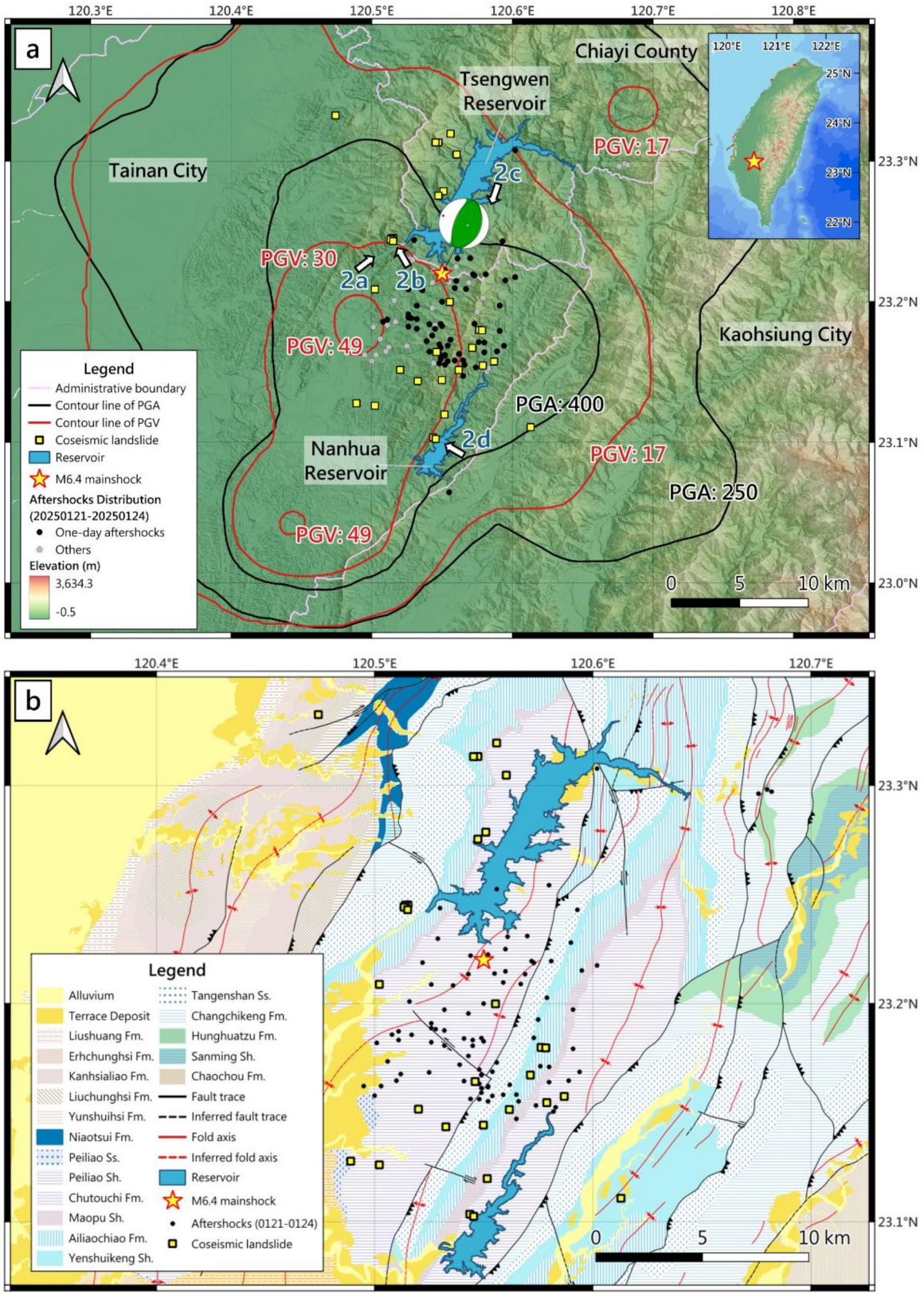

Fig. 1 (See legend on next page.)

(See figure on previous page.)

Fig. 1 Distribution of the coseismic landslides of the 2025 M6.4 Dapu earthquake. **a** Relationship between coseismic landslides and ground motions. The contour line of PGA and PGV is derived from Wu et al. (2025). Yellow squares represent the location of the 29 coseismic landslides from the ARDSWC. White arrows indicate the looking direction and location of the field photos. **b** 1:50,000 Geological Maps of Taiwan's river basins (2013) in southwestern Taiwan. Black lines represent fault traces and red lines are fold axes. Dashed lines indicate the inferred traces or axes. Fm. is the abbreviation of formation; Sh. is shale; Ss. is sandstone

Lombardo 2019). To mitigate the potential geological hazard following an earthquake, it is important to accurately identify the location of each landslide and monitor regions at high risk of further landsliding, especially during the rainy season. Additionally, recent studies (Hailemikael et al. 2016; Rault et al. 2020) point out the critical role of geological conditions in determining the response of mountainous terrain to seismic shaking.

In this fast report, we utilize the coseismic landslides inventory of the Dapu earthquake compiled by the Agency of Rural Development and Soil and Water Conservation (ARDSWC) to investigate key triggering factors of the coseismic landslides. A field survey was also conducted to assess the in-situ conditions of severely affected mountainous areas, with the aim of proving recommendations for hazard mitigations.

1.1 Data analysis process

To detect coseismic landslides associated with the Dapu earthquake, the ARDSWC used the pre-event Sentinel-2 (Date: Dec. 20, 2024) and post-event PlanetScope (Date: Jan. 21, 2025) and Sentinel-2 (Date: Jan. 24, 2025) satellite imagery. The mainshock information and the aftershocks catalog (Jan. 21 to Jan. 24) were obtained from the CWA website, while the mainshock focal mechanism was achieved from AutoBATS CMT Catalog (Jian et al. 2018; Heidbach et al. 2022). The Peak Ground Acceleration (PGA) and Peak Ground Velocity (PGV) values are based on Wu et al. (2025). Average slope and slope aspect for each landslide were derived using the "zonal statistics" function built in QGIS with 5-m resolution DEM data from the Department of Land Administration (DLA). Additional factors such as lithology (e.g. Henriques et al. 2015), dip slopes (e.g. Guzzetti et al. 2008), historic landslides (e.g. Martino et al. 2022; Wei et al. 2024) were also considered. We consulted the 1:50,000 Geological Maps of Taiwan's river basins (2013), and used QGIS WMS/WMTS layers from the GSMMA to determine the geological context and whether the landslides were located on dip slopes or within historic landslides zones.

1.2 Spatial distribution of coseismic landslides

The ARDSWC detected 29 coseismic landslides with a total area around 101,550 m^2 in this event. Among these landslides, 11 occurred north of the epicenter, while 18 were located to the south. In other words, about two-thirds of the coseismic landslides were concentrated in the southern region (Fig. 1), suggesting that the fault rupture likely propagated southward. Such directional propagation may have produced stronger ground motions in the southern area due to the directivity effect, resulting in the concentration of the coseismic landslides (Marc et al. 2017; Li et al. 2024). The distribution of these landslides clustered in the southwestern region, indeed corresponding to the areas with the largest coseismic slip (Lee et al. 2025a, b) and the strongest ground shaking (Wu et al. 2025).

Figure 1a shows that all the coseismic landslides occurred in areas experiencing PGA over 250 cm/s^2, and 22 were in areas where PGA exceeded 400 cm/s^2. Regarding PGV, all 29 landslides occurred when PGV exceeded 17 cm/s, with 8 exceeding 30 cm/s. These findings are consistent with Chang et al. (2024), who found that landslides triggered by the 2024 Hualien earthquake were mainly concentrated in regions with PGA over 250 cm/s^2 and PGV over 15 cm/s (i.e., the upper bound of seismic intensity level 5 + in Taiwan and the lower bound of seismic intensity level 5- respectively). Our field surveys also revealed that several small-sized landslides occurred in areas with PGA exceeded 250 cm/s^2 and PGV above 17 cm/s, as well as many fresh landslides (scarps) below the detection limit of satellite imagery in areas with PGA exceeded 400 cm/s^2 and PGV was around 30 cm/s (Fig. 2).

1.3 Analysis of coseismic landslides

In addition to the spatial distribution of coseismic landslides, we also analyzed the geological and geomorphological factors that influence landslides including lithology, slope degree, slope aspect, dip slope and historic landslides (Table 1; Fig. 3). In terms of lithology, the landslides occurred across 7 different geological formations (Fig. 1b), based on stratigraphy from Shao and Kao (2009): Miocene to Early Pliocene Tangenshan Sandstone (Tn), Pliocene Yenshuikeng Shale (Ys), Pliocene Ailiaochiao Formation (Al), Pliocene Maopu Shale (Mp), Late Pliocene to Pleistocene Chutouchi Formation (Ct), Pleistocene Peiliao Shale (Pa), and Pleistocene Liuchunghsi Formation (Lu). However, no clear relationship between lithology and landslide distribution was observed (Fig. 3a). Based on the Vs30 values from Chen et al. (2022), all formations fall under the NEHRP category of dense soil and soft rock, suggesting that the variations in rock strength may not significantly affect landslide susceptibility in this region.

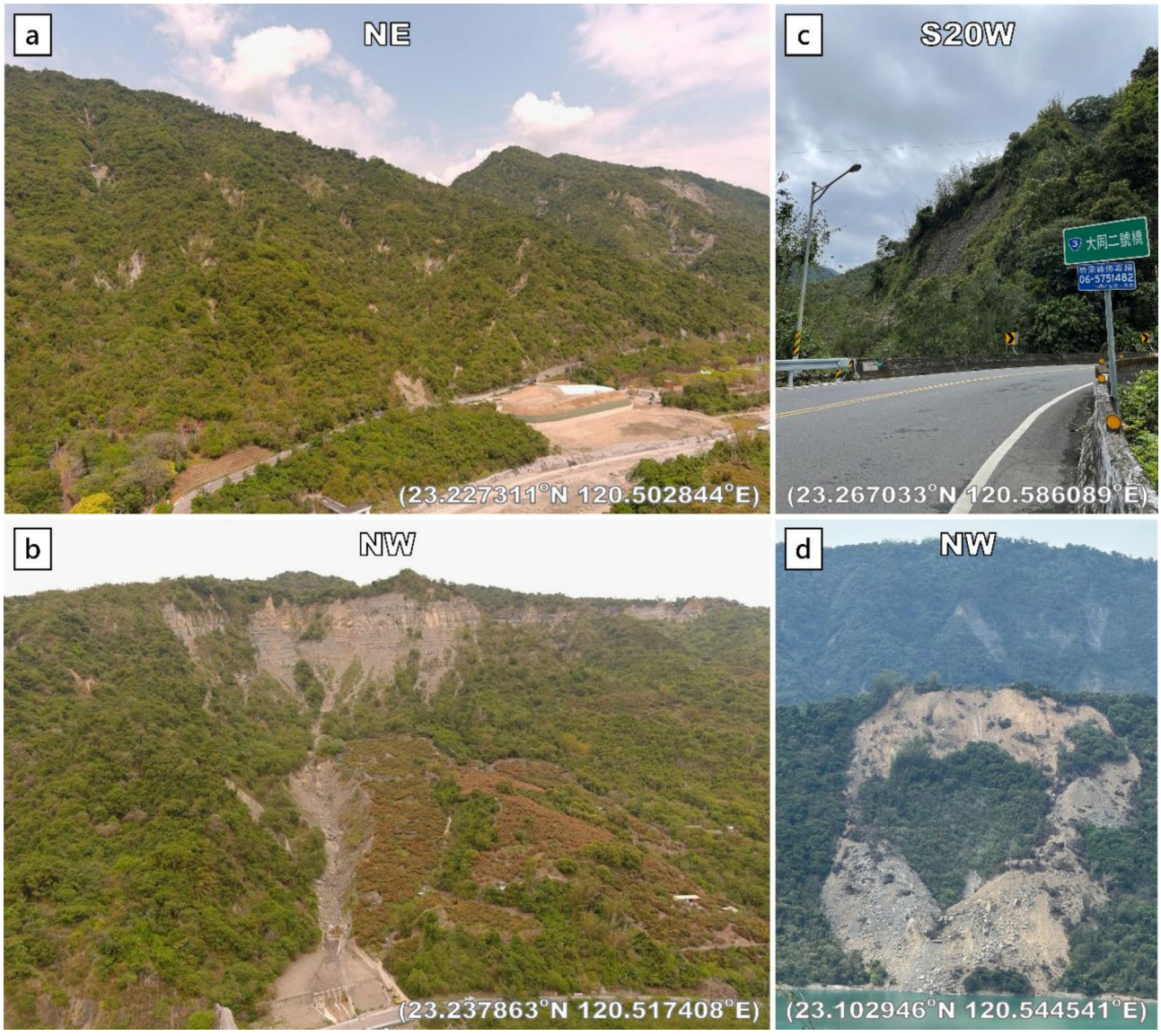

Fig. 2 Field photos of areas highly affected by the Dapu earthquake. **a** Numerous fresh landslides (scarps) develop in southwestern mountainous regions of Tsengwen Reservoir where PGA exceeded 400 cm/s^2 and PGV was around 30 cm/s **b** Coseismic landslides near the tourist center of Tsengwen Reservoir. **c** Local coseismic landslide cannot be detected from satellite imagery. We observed quite a few small-sized landslides in the boundary of PGV between 17 to 30 cm/s during the field survey. **d** Two of the largest coseismic landslides next to the Nanhua Reservoir

Slope gradient analysis revealed that only 3 landslides have an average slope lower than 20°, while the majority occurred on slopes ranging from 30° to 50°, and even 5 had slopes exceeding 50° (Fig. 3b). This distribution is consistent with the findings from the Chi-Chi earthquake in 1999 (Lin et al. 2004, 2006), showing that coseismic landslides tend to occur on steeper slopes, unlike rain-induced landslides. As ground motion amplification is expected to occur at ridge crests due to topographic site effect (e.g. Geli et al. 1988; Meunier et al. 2008; Hartzell et al. 2014; Khan et al. 2020), which explains the coseismic landslides distribution regarding the slope degrees.

With respect to slope aspect, most landslides occurred on southeast- to southwest-facing slopes, with none on north- or northwest- facing slopes (Fig. 3c). Previous studies suggest that slopes facing away from the epicenter experience greater shaking (e.g. Meunier et al. 2008; Chen et al. 2019; Khan et al. 2020). Nonetheless, our findings only partially align with theirs: in the southern region, southeast-facing slopes dominate, but in the northern areas, coseismic landslides also mainly occurred on the south-facing slopes oriented toward the epicenter. In fact, Hartzell et al. (2014) demonstrated that ground motions can be amplified in areas aligned with the incoming seismic waves, regardless of whether the

Table 1 Information of 29 coseismic landslides detected from satellite imagery before and after the Dapu earthquake

No.[a]	Landslide Area (m^2)	E	*N*	PGA[b] (cm/s^2)	PGV[b] (cm/s)	Lithology[c]	Avg. Slope (degree)	Avg. Aspect	Dip Slopes	Historic Landslides
1	1049.0	120.474	23.333	250–400	17–30	Lu	43.1 ± 7.2	163.3 ± 23.6	no	yes
2	3696.7	120.556	23.319	250–400	17–30	Mp	37.3 ± 5.0	56.4 ± 20.9	no	yes
3	1848.3	120.547	23.313	250–400	17–30	Al	55.5 ± 3.6	193.6 ± 7.9	no	yes
4	2297.9	120.545	23.313	250–400	17–30	Al	56.8 ± 12.0	183.8 ± 21.4	no	yes
5	1149.0	120.560	23.305	250–400	17–30	Ct	49.8 ± 7.6	219.5 ± 6.8	no	yes
6	2148.1	120.551	23.279	250–400	17–30	Ct	47.3 ± 7.1	223.6 ± 8.8	no	yes
7	1198.9	120.547	23.275	250–400	17–30	Al	53.0 ± 3.0	222.2 ± 9.2	no	no
8	5395.0	120.515	23.245	> 400	17–30	Tn	35.8 ± 9.5	180.7 ± 11.9	no	yes
9	1148.9	120.514	23.245	> 400	17–30	Tn	30.6 ± 3.2	176.0 ± 4.1	no	yes
10	2397.8	120.513	23.244	> 400	17–30	Tn	34.3 ± 4.8	114.4 ± 18.8	no	yes
11	2947.2	120.515	23.243	> 400	17–30	Tn	11.4 ± 7.1	144.6 ± 65.6	no	yes
12	2447.7	120.502	23.209	> 400	30–49	Ct	46.0 ± 9.7	235.8 ± 30.8	no	yes
13	3147.2	120.555	23.200	> 400	30–49	Pa	29.9 ± 7.5	260.8 ± 38.2	no	yes
14	1761.7	120.576	23.180	> 400	17–30	Al	49.4 ± 4.7	134.2 ± 8.0	yes	no
15	2116.8	120.578	23.180	> 400	17–30	Al	41.0 ± 7.3	156.9 ± 23.4	yes	yes
16	3204.9	120.571	23.167	> 400	17–30	Al	42.2 ± 5.9	123.0 ± 19.9	yes	no
17	1049.1	120.546	23.164	> 400	30–49	Ct	52.6 ± 16.2	166.2 ± 28.5	no	yes
18	1598.6	120.587	23.157	> 400	17–30	Pa	41.0 ± 20.4	235.1 ± 31.8	no	yes
19	1598.6	120.579	23.155	> 400	17–30	Ct	25.4 ± 12.8	198.3 ± 74.8	no	yes
20	1108.4	120.520	23.152	> 400	30–49	Ct	45.6 ± 5.0	100.7 ± 7.1	no	yes
21	1204.4	120.562	23.151	> 400	17–30	Al	47.7 ± 2.4	116.4 ± 4.2	yes	yes
22	1085.1	120.550	23.144	> 400	30–49	Tn	57.3 ± 2.2	128.4 ± 5.7	yes	yes
23	6743.8	120.533	23.144	> 400	30–49	Ct	32.0 ± 4.6	202.5 ± 22.4	no	no
24	2643.7	120.489	23.128	> 400	30–49	Pa	32.6 ± 5.6	134.5 ± 22.5	no	no
25	1325.8	120.502	23.126	> 400	30–49	Pa	14.2 ± 7.5	106.1 ± 51.6	no	no
26	3125.5	120.552	23.120	> 400	17–30	Mp	42.3 ± 10.7	131.1 ± 40.4	no	yes
27	1598.7	120.613	23.111	> 400	17–30	Ys	12.5 ± 1.9	47.8 ± 10.3	no	no
28	13537.7	120.544	23.103	> 400	17–30	Ct	33.2 ± 5.3	132.3 ± 23.3	yes	yes
29	26975.5	120.545	23.102	> 400	17–30	Ct	31.8 ± 3.0	123.5 ± 28.9	yes	yes

[a] This table is arranged from north to south; Landslides No. 1–11 locate in the north of the epicenter

[b] The value of PGA and PGV is from Wu et al. (2025)

[c] See text for the full name of the rock formation's abbreviation

slope faces toward or away from the epicenter, which may explain our observations.

Apart from the interaction between incoming direction of seismic waves and slope's facing direction, pre-existing weak surface is also an important factor. Guzzetti et al. (2008) noted that landslides are more common with dip slopes in areas where rocks are regularly bedded. The catalog of dip slopes from the GSMMA shows numerous dip slopes located in this region, while the geological profiles from Le Béon et al. (2024) show the presence of a series of anticlines and synclines. Therefore, we infer that the dip slope is a critical triggering factor in this area. The spatial intersection between coseismic landslides and the catalog reveals that 7 coseismic landslides were spatially associated with dip slopes, accounting for nearly half of the total landslide area (Fig. 3d), highlighting the role of dip slope in landslide triggering. Finally, historic landslides also found to play a significant role (e.g. Martino et al. 2022; Wei et al. 2024), as 75% of the mapped landslides overlapped with historical landslide areas. This indicates that the reactivation of pre-existing failures is also a key mechanism (Fig. 3d).

1.4 Hazard mitigation plans

Compared to landslides inventories worldwide (e.g. Malamud et al. 2004; Tiwari et al. 2017), the number of coseismic landslides triggered by Dapu earthquake is slightly lower than those associated with earthquakes of similar magnitude. However, our field surveys revealed that some fresh landslide scarps are below the resolution of satellite images (Fig. 2a and c), indicating the actual number may be underestimated. Previous studies have shown that seismic shaking can have legacy effects in mountainous areas, as it temporarily lowers threshold for triggering landslide (e.g. Shieh et al. 2009; Hovius et al., 2011; Tanyaş et al. 2021), even from M5-6 earthquake events (Martino et al. 2022). Furthermore, strong ground motions can alter slope deformation behavior (He et al.

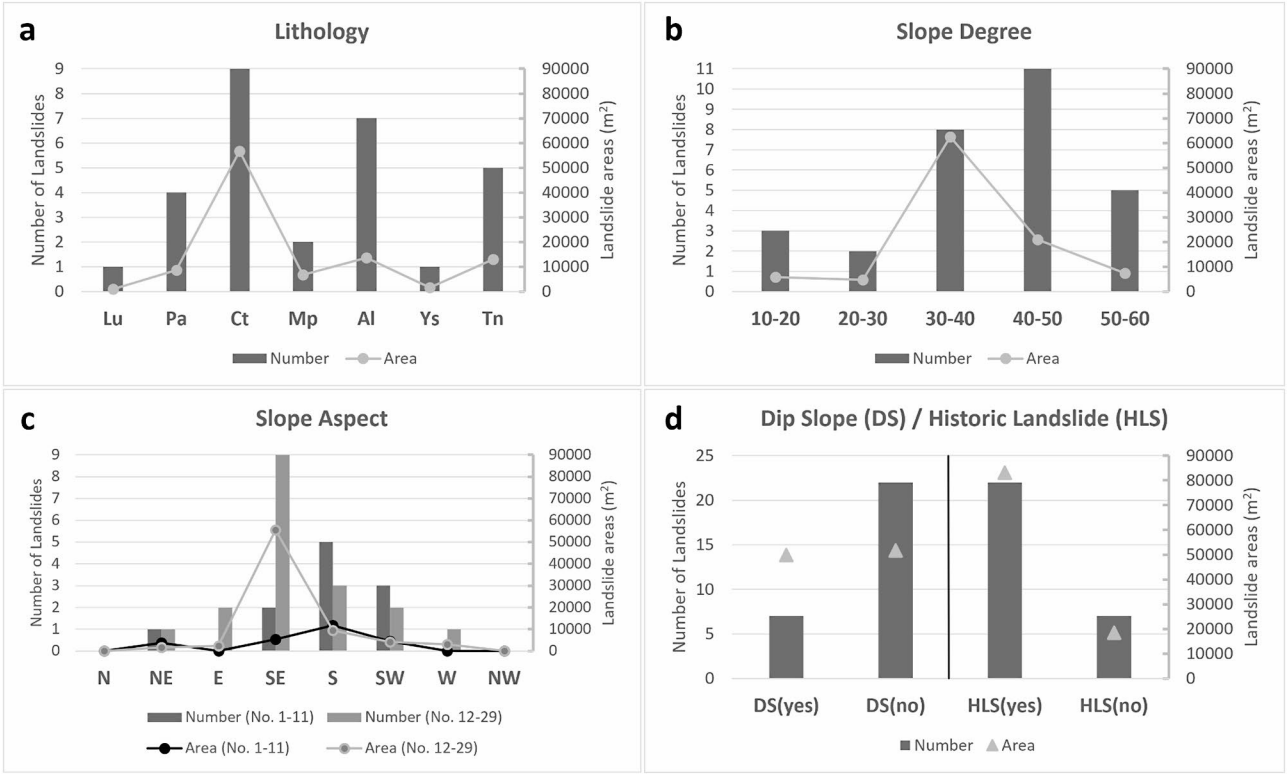

Fig. 3 Relationship between critical factors, numbers and areas of coseismic landslides. **a** Lithology: Landslide count and affected area across seven geological formations—Lu: Liuchunghsi Formation, Pa: Peiliao Shale, Ct: Chutouchi Formation, Mp: Maopu Shale, Al: Ailiaochiao Formation, Ys: Yenshuikeng Shale, Tn: Tangenshan Sandstone. **b** Slope degree: Distribution of landslide number and area across five slope categories (in degrees). **c** Slope aspect: Comparison of landslides north (No. 1–11) and south (No. 12–29) of the epicenter by aspect direction; bars represent number of landslides, and lines show cumulative landslide area (Table 1). **d** Dip slopes / Historic landslides: Number and area of landslides associated with dip slopes (DS) and historic landslides (HLS); "yes" indicates spatial overlap with catalog data

2024). The regions surrounding the Tsengwen and Nanhua Reservoirs (Fig. 3) were both highly affected by the Dapu earthquake and now be in a destabilized state. If the threshold for triggering landslides and debris flows decreased, the functionality of these reservoirs could be severely affected during the wet season, posing further risks to the residents in this region. As a result, detailed landslides mapping is essential to provide key information for hazard mitigation plans and minimize the impact of further geological hazards in southwestern Taiwan, during the coming rainy season.

2 Summary

The M6.4 Dapu earthquake likely ruptured southward, causing stronger shaking and more landslides in the southern region. Most coseismic landslides occurred in areas where PGA exceeded 250 cm/s^2 and PGV was higher than 17 cm/s. Field observations also identified fresh landslide scarps in areas with PGA over 400 cm/s^2 and PGV around 30 cm/s, which were not detected by satellite imagery. Topographic site effect contributed to the distribution of landslides along the ridge crests, especially on slopes ranging from 30° to 50°. Dip slopes and reactivated historic landslides were also major factors contributing to the occurrence of coseismic landslides. These findings provide critical insights into landslide triggering mechanisms and support the need for detailed landslides mapping and advanced hazard mitigation plans in anticipation of the upcoming rainy season.

Acknowledgements
We gratefully appreciate Wen-Ting Yeh, Chun-Ting Chen, Che-Yu Li, Wei-Chen Huang, and Dong-Yang Chen for their assistance in the field survey.

Author contributions
Y.-Y.L. wrote the main manuscript. C.-E.L. assisted in the interpretation of the results. C.-Y.C. approved the final manuscript. All authors reviewed the manuscript.

Data availability
Coseismic landslides inventory of the Dapu earthquake can be accessed through ARDSWC's BigGIS website at https://gis.ardswc.gov.tw/map/. The information of the Dapu earthquake and its aftershocks can be downloaded from CWA website at https://scweb.cwa.gov.tw/zh-tw/earthquake/data. The focal mechanism can be achieved from AutoBATS CMT Catalog website at https://tecdc.earth.sinica.edu.tw/FM/AutoBATS/. The 1:50,000 Geological Maps of Taiwan's river basins (2013), the Catalog of dip slopes and the Catalog of historic landslides from GSMMA can be accessed as WMS/WMTS layer using (1) https://geomap.gsmma.gov.tw/mapguide/mapagent/mapagent.fcgi?; (2) https://landslide.geologycloud.tw/jlwmts/jetlink/wmts.

Declarations

Competing interests

The authors declare no competing interests.

Received: 27 February 2025 / Accepted: 13 April 2025
Published online: 18 April 2025

References

Chang J-M, Chao W-A, Yang C-M, Huang M-W (2024) Coseismic and subsequent landslides of the 2024 Hualien earthquake (M7.2) on April 3 in Taiwan. Landslides 21:2591–2595. https://doi.org/10.1007/s10346-024-02312-x

Chen Y-C, Chang K-T, Wang S-F, Huang J-C, Yu C-K, Tu J-Y, Chu H-J, Liu C-C (2019) Controls of Preferential orientation of earthquake- and rainfall-triggered landslides in Taiwan's orogenic mountain belt. Earth Surf Proc Land 44(9):1661–1674

Chen C-T, Kuo C-H, Lin C-M, Huang J-Y, Wen K-L (2022) Investigation of shallow S-wave velocity structure and site response parameters in Taiwan by using high-density microtremor measurements. Eng Geol 297:106498. https://doi.org/10.1016/j.enggeo.2021.106498

Geli L, Bard PY, Jullien B (1988) The effect of topography on earthquake ground motion: a review and new results. Bull Seismol Soc Am 78(1):42–63. https://doi.org/10.1785/BSSA0780010042

Guzzetti F, Ardizzone F, Cardinali M, Galli M, Reichenbach P, Rossi M (2008) Distribution of landslides in the upper Tiber river basin, central Italy. Geomorphology 96(1–2):105–122. https://doi.org/10.1016/j.geomorph.2007.07.015

Hailemikael S, Lenti L, Martino S, Paciello A, Rossi D, Scarascia Mugnozza G (2016) Ground-motion amplification at the Colle Di Roio ridge, central Italy: a combined effect of stratigraphy and topography. Geophys J Int 206(1):1–18. https://doi.org/10.1093/gji/ggw120

Hartzell S, Meremonte M, Ramírez-Guzmán L, McNamara D (2014) Ground motion in the presence of complex topography: earthquake and ambient noise sources. Bull Seismol Soc Am 104(1):451–466. https://doi.org/10.1785/0120130088

He K, Lombardo L, Chang L, Sadhasivam N, Hu X, Fang Z, Dahal A, Fadel I, Luo G, Tanyas H (2024) Investigating earthquake legacy effect on hillslope deformation using InSAR-derived time series. Earth Surf Proc Land 49(3):980–990. https://doi.org/10.1002/esp.5746

Heidbach O, Liang W-T, Morawietz S, von Specht S, Ma K-F, GFZ German Research Center for Geosciences (2022) Stress map of Taiwan 2022. https://doi.org/10.5880/WSM.Taiwan2022

Henriques C, Zêzere JL, Marques F (2015) The role of the lithological setting on the landslide pattern and distribution. Eng Geol 189:17–31. https://doi.org/10.1016/j.enggeo.2015.01.025

Hovius N, Meunier P, Lin C-W, Chen H, Chen Y-G, Dadson S, Horng M-J, Lines M (2011) Pro-longed seismically induced erosion and the mass balance of a large earthquake. Earth Planet Sci Lett 304(3–4):347–355. https://doi.org/10.1016/j.epsl.2011.02.005

Jian P-R, Tseng T-L, Liang W-T, Huang P-H (2018) A new automatic full waveform regional moment tensor inversion algorithm and its applications in the Taiwan area. Bullentin Seismological Soc Am 108(2):573–587. https://doi.org/10.1785/0120170231

Keefer DK (1984) Landslides caused by earthquakes. Geol Soc Am Bull 95:406–421

Khan S, Van Der Meijde M, Van Der Werff H, Shafique M (2020) The impact of topography on seismic amplification during the 2005 Kashmir earthquake. Nat Hazards Earth Syst Sci 20(2):399–411. https://doi.org/10.5194/nhess-20-399-2020

Le Béon M, Chen C-C, Huang W-J, Ching K-E, Shih J-W, Tseng Y-C, Chiou Y-W, Liu Y-C, Hsieh M-L, Pathier E, Lu C-H, Fruneau B (2024) Aseismic deformation within fold-and-thrust belts: example from the Tsengwen river section of Southwest Taiwan. Geoscience Lett 11(1):57. https://doi.org/10.1186/s40562-024-00373-3

Lee S-J, Liu T-Y, Lin T-C (2025a) Fast report: source rupture model analysis of the 2025 Dapu earthquake, Taiwan. Terrestrial. Atmospheric Ocean Sci 36:13. https://doi.org/10.1007/s44195-025-00098-6

Lee Z, Chuang RY, Wang I-T, Chen L, Chang W-L, Chiu C-Y, Ching K-E, Guo S-W, Chen C-L (2025b) Fast report: surface deformation associated with the 2025 Dapu earthquake. Terr Atmospheric Ocean Sci 36:11. https://doi.org/10.1007/s44195-025-00090-0

Li Z, Chen G, Han Z, Hazarika H, Xia M, Feng C (2024) The influence of pulse-like ground motion caused by the directivity effect on landslide triggering. Bull Eng Geol Environ 83(1):48. https://doi.org/10.1007/s10064-023-03514-8

Lin C-W, Shieh C-L, Yuan BD, Shieh Y-C, Liu S-H, Lee S-Y (2004) Impact of Chi-Chi earthquake on the occurrence of landslides and debris flows: example from the Chenyulan river watershed, Nantou, Taiwan. Eng Geol 71:49–61. https://doi.org/10.1016/S0013-7952(03)00125-X

Lin C-W, Liu S-H, Lee S-Y, Liu C-C (2006) Impacts of the Chi-Chi earthquake on subsequent rainfall-induced landslides in central Taiwan. Eng Geol 86(2–3):87–101. https://doi.org/10.1016/j.enggeo.2006.02.010

Malamud BD, Turcotte DL, Guzzetti F, Reichenbach P (2004) Landslide inventories and their statistical properties. Earth Surf Proc Land 29:687–711. https://doi.org/10.1002/esp.1064

Marc O, Meunier P, Hovius N (2017) Prediction of the area affected by earthquake-induced landsliding based on seismological parameters. Nat Hazards Earth Syst Sci 17:1159–1175. https://doi.org/10.5194/nhess-17-1159-2017

Martino S, Fiorucci M, Marmoni GM, Casaburi L, Antonielli B, Mazzanti P (2022) Increase in landslide activity after a low-magnitude earthquake as inferred from DInSAR interferometry. Sci Rep 12(1):2686. https://doi.org/10.1038/s41598-022-06508-w

Meunier P, Hovius N, Haines JA (2008) Topographic site effects and the location of earthquake induced landslides. Earth Planet Sci Lett 275(3–4):221–232. https://doi.org/10.1016/j.epsl.2008.07.020

Rault C, Chao W-A, Gelis C, Burtin A, Chang J-M, Marc O, Lai T-S, Wu Y-M, Hovius N, Meunier P (2020) Seismic response of a mountain ridge prone to landsliding. Bull Seismol Soc Am 110(6):3004–3020. https://doi.org/10.1785/0120190127

Shao P-H, Kao M-C (2009) Geological map of Taiwan scale 1:50,000, Zhongpu Sheet. (in Chinese)

Shieh C-L, Chen Y-S, Tsai Y-J, Wu J-H (2009) Variability in rainfall threshold for debris flow after the Chi-Chi earthquake in central Taiwan, China. Int J Sedim Res 24(2):177–188. https://doi.org/10.1016/S1001-6279(09)60025-1

Tanyaş H, Lombardo L (2019) Variation in landslide-affected area under the control of ground motion and topography. Eng Geol 260:105229. https://doi.org/10.1016/j.enggeo.2019.105229

Tanyaş H, Kirschbaum D, Görüm T, van Westen CJ, Tang C, Lombardo L (2021) A closer look at factors governing landslide recovery time in post-seismic periods. Geomorphology 391:107912. https://doi.org/10.1016/j.geomorph.2021.107912

Tiwari B, Ajmera B, Dhital S (2017) Characteristics of moderate-to large-scale landslides triggered by the M W 7.8 2015 Gorkha earthquake and its aftershocks. Landslides 14:1297–1318. https://doi.org/10.1007/s10346-016-0789-0

Wei T, Xia M, Zhang X, Qi S (2024) Investigating the reactivation of historical landslides during the 2022 Luding MS6.8 earthquake. Earthq Sci 37(3):200–209. https://doi.org/10.1016/j.eqs.2024.03.002

Wu Y-M, Lin Y-H, Yang BM, Ke S-S (2025) Performance of the P-alert real-time shakemaps system and onsite warning during the 2025 ML6. 4 Dapu earthquake. Terr Atmospheric Ocean Sci 36:3. https://doi.org/10.1007/s44195-025-00086-w

Publisher's note